Modeling and Analysis of the Uplink Local Delay in MEC-Based VANETs

Yuying Wu and Jun Zheng, *Senior Member, IEEE*

***Abstract*—Mobile edge computing (MEC) is a new computing paradigm for addressing users' ever-increasing demand for quality of service (QoS) in vehicular ad hoc networks (VANETs). The local delay is a performance metric that has a big impact on the QoS provisioned to users. This paper studies the analysis of the local delay in an MEC-based VANET based on stochastic geometry. An analytical model is first derived to analyze the average uplink local delay of a vehicle on a highway for sending a packet to an edge node along the highway. In deriving the model, the spatial distributions of vehicles and edge nodes are modeled as an independent one-dimensional (1-D) homogeneous Poisson point process (PPP). The edge node for accommodating the service request of a vehicle node is determined based on a nearest-receiver model. Moreover, a carrier sense multiple access (CSMA) mechanism is considered for channel access in the derived local delay model. The derived analytical model is validated through simulation results and the impacts of major parameters on the average uplink local delay are investigated. The derived model can be used to provide a basis for parameter settings in the deployment of edge nodes.**

***Index Terms*—Mobile edge computing, MEC, stochastic geometry, local delay, VANET.**

I. Introduction

With the emergence of new applications in vehicular ad hoc networks (VANETs), vehicular users have an increasing demand for quality of service (QoS) with low latency and high reliability [1]–[5]. Mobile edge computing (MEC) has been considered as a computing paradigm that can bring several benefits, such as QoS provisioning and task offloading [6]–[14]. MEC is a type of distributed cloud computing, in which small computing servers called MEC servers are deployed on the road or edge side so that a delay-sensitive service can be provisioned closer to the user side. The main components of an MEC-based VANET include roadside units (RSUs) and MEC servers. Normally, an MEC server is locally associated with an RSU, and an RSU together with its associated MEC server is referred to as an edge node.

Delay is one of the most important metrics to measure the QoS of a network. In general, the delay for successfully transmitting data from one node to another node consists of several components, including the processing delay, access delay, propagation delay, and local delay over a link. The local delay is defined as the time taken to successfully transmit a packet over a link, which depends on the number of retransmissions of a packet over a link [15]. A retransmission over a link can be caused by an unsuccessful channel access of a node or small receiving power of the transmission signal at a receiving node. Obviously, a larger local delay would lead to a larger overall delay for successfully transmitting a packet, which may cause untimely completion of a requested service. In particular, the local delay could be infinite under certain network parameters [15], which would cause the failure of a requested service. Therefore, it is important to analyze the impact of network parameters on the local delay in order to reduce the local delay and thus timely complete a requested service.

In this paper, we study the analysis of the local delay in an MEC-based VANET and consider the uplink local delay of a vehicle requesting for the computing service of an edge node in a highway scenario. An analytical model is first derived based on stochastic geometry for analyzing the average uplink local delay of a vehicle driving on a highway for sending a packet to an edge node along the highway. In deriving the analytical model, the spatial distribution of vehicle nodes on each lane and that of edge nodes are modeled as an independent 1-D homogeneous Poisson point process (PPP), respectively. A nearest-receiver model is used to determine the edge node for accommodating the service request of a vehicle node. Moreover, unlike most existing models, the derived local delay model considers a carrier sense multiple access (CSMA) mechanism for channel access, which is more typical for a VANET. The derived analytical model is validated through simulation results and the impacts of major parameters on the local delay are investigated.

The main contributions of this paper include the following aspects:

1) A closed-form expression of the uplink local delay is derived for an MEC-based VANET;
2) The impact of a CSMA mechanism on the uplink local delay is studied;
3) The effects of major network parameters on the uplink local delay are investigated based on the derived local delay model;
4) The derived local delay model can be used to provide a basis for parameter settings in the deployment of edge nodes.

Manuscript received May 7, 2019; revised October 11, 2019 and January 23, 2020; accepted January 26, 2020. Date of publication January 30, 2020; date of current version April 16, 2020. This work was supported in part by the National Key R&D Program of China under Grant 2018YFB1800801, and in part by the National Natural Science Foundation of China under Grant 61771131. The review of this article was coordinated by Dr. J. Liu.*(Corresponding author: Jun Zheng.)*

The authors are with the National Mobile Communications Research Laboratory, Southeast University, Nanjing 210096, China (e-mail: yuyingwu@seu.edu.cn; junzheng@seu.edu.cn).

Digital Object Identifier 10.1109/TVT.2020.2970551

The remainder of the paper is organized as follows. Section II reviews related work in the literature. Section III describes the system model. Section IV presents the derived local delay model. Section V shows numerical results to validate the derived model and investigate the impact of major parameters on the uplink local delay. Section VI concludes this paper.

II. Related Work

The local delay has been studied in the literature [16]–[22]. In [16], Haenggi derived the local delay of a 2-D Poisson network with slotted ALOHA. In deriving the local delay, four different transmission models are considered, including the nearest-receiver transmission (NRT) model, the nearest-neighbor transmission (NNT) model, the nearest-transmitter reception (NTR) model, and the nearest-neighbor reception (NNR) model. But the spatial distribution of the nodes is modeled as a homogeneous 2-D PPP. In [17], Gong and Haenggi analyzed the local delay in a Poisson network under the finite motion model based on [16]. In the considered network model, however, each node has a home location and a mobility region, and makes a displacement in any direction in a timeslot within the mobility region with a given probability. Thus, the derived local delay model is not suitable for a highway scenario. In [18], Nie *et al.* analyzed the local delay of a transmission between a cellular downlink user and a BS in a heterogeneous cellular network (HetNet). The network has several independent tiers, where BSs with different transmitting power are deployed with different densities and path-loss exponents. However, the considered network model is not suitable for an MEC-based VANET. In [19], Salehi *et al.* studied the signal-to-interference ratio (SIR) meta distribution of device-to-device (D2D) underlaid cellular networks, where the spatial distributions of D2D transmitters and base stations are modeled as Poisson point processes (PPPs). The local delay of a transmission between D2D users and a transmission between a BS and a cellular downlink user with an ALOHA-type channel access mechanism were derived based on the meta distribution. Each D2D transmitter has a corresponding D2D receiver at a given distance, and each cellular downlink user receives a packet from its nearest BS. However, the D2D underlaid cellular network is quite different from an MEC-based VANET, and the assumption that each transmitter has a dedicated receiver located at a given distance in a random direction is not practical in an MEC-based VANET. In [20], Liu *et al.* derived the local delay in a Poisson network with a coordinated transmission mechanism. In the coordinated transmission mechanism, several transmitters send the same signal to a considered receiver. However, the coordinated transmission mechanism is not suitable for MEC-based VANET, where a service request vehicle node sends a packet to its nearest edge node. In [21], Haenggi presented the local delay of a transmission between two neighboring nodes in a static network and a mobile Poisson network with ALOHA, respectively. The spatial distribution of all nodes in the networks follows a 2-D PPP. However, the considered network model is not an MEC-based VANET. In [22], Dong *et al.* analyzed the local delay of a transmission between a mobile user with infinite mobility and its nearest BS in HetNets. A Poisson cluster point process (PCP) is used to describe the spatial distribution of the BSs at each tier with a certain coverage radius. In an MEC-based VANET, however, the vehicle nodes and edge nodes are not randomly distributed in a 2-D plane but along a road. Thus, the positions of vehicle nodes and edge nodes cannot be modeled randomly as a cluster in a circle with a certain radius. The derived model cannot describe the local delay in an MEC-based VANET.

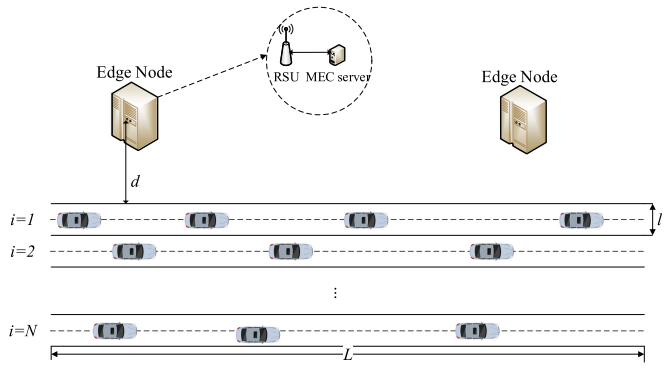

Fig. 1. Network scenario.

Compared with all the above work, this work considers an MEC-based VANET, which is different from a regular 2-D Poisson network and a cellular network. Moreover, we use an independent 1-D homogeneous PPP to model the spatial distribution of vehicle nodes and that of edge nodes, and consider a carrier sense multiple access (CSMA) mechanism for channel access, which are different from the existing work.

III. System Model

In this section, we describe the system model considered in this paper.

A. Network Scenario

We consider a highway road with N one-way lanes of length L, as shown in Fig. 1. The N lanes are numbered by $i = 1, 2, \ldots, N$. The width of each lane is l. A certain number of RSUs are deployed along the road. For each RSU, there is a locally associated MEC server. An RSU and its associated MEC server constitute an edge node. For ease of exposition, we assume that all the edge nodes are deployed on a virtual lane along the road, and the virtual lane is numbered by $i = 0$. The perpendicular distance between an edge node and its nearest lane is d. When a vehicle node needs the service of an MEC server, it will first send a service request to an edge node. After receiving the request, the edge node will perform computing, and then send the computing result to the requesting vehicle node.

B. Assumptions

For the network scenario in Fig. 1, we make the following assumptions:

1) *Spatial Distribution:* The spatial distribution of edge nodes follows a homogeneous Poisson point process (PPP) with density λ_e, which is denoted by Φ_e. The spatial distribution of the vehicle nodes on each lane follows

an independent homogeneous PPP, which is denoted by $\Phi_v^i (i = 1, 2, \ldots, N)$. The density of the vehicle nodes on each lane is λ_v^i. The spatial distribution of the vehicle nodes on all lanes is denoted by $\Phi_v = \{\Phi_v^1, \Phi_v^2, \ldots, \Phi_v^N\}$.

2) *Nearest-Receiver Model:* A service requesting node selects the "serving edge node" to receive its data packets based on the nearest-receiver model [23]. In the nearest-receiver model, the potential receivers for a particular transmitter form a stationary point process, and the transmitter can only select the nearest receiver (i.e., in a listening state) to receive its data packets. Here, the edge node that is in a listening state and is closest to the service requesting node is referred to as a serving edge node.
3) *Channel Fading:* The power fading coefficient between two nodes, denoted by $h_{x,y}$, is exponentially distributed with mean 1 (Rayleigh fading), where *x* and *y* denote the positions of the two nodes, respectively. Different fading coefficients are independent of each other. The large-scale path loss between two nodes is estimated by $d_{x,y}^{-\alpha} = \|x - y\|^{-\alpha}$, where $d_{x,y}$ denotes the Euclidean distance between node *x* and node *y*, and $\alpha (\alpha > 2)$ is the path loss exponent. Like in [18], [24], we neglect the effect of thermal noise and focus on the interference-limited case.
4) *Transmission Power:* The transmission power of each edge node is equal. The transmission power of each vehicle node is equal.
5) *Channel Access:* Time is equally divided into a sequence of timeslots. In each timeslot, a CSMA mechanism is employed for channel access contention. For each node, there is a contention domain. The condition that node *y* falls in the contention domain of node *x* is that the transmission power detected at node *x* from node *y* is beyond a certain threshold. A node in the contention domain of node *x* is called a neighbor of node *x*. Each node in channel contention via CSMA will initiate a timer with a random value, which follows an independent uniform distribution between 0 and 1. Once the timer times out, the node will transmit its packet. Therefore, to successfully access a channel, i.e., successfully transmit a packet over a link, a node must meet one of the two conditions in the slot: 1) there is no neighbor in its contention domain; 2) there are neighbors in its contention domain but the timer values of all neighbors are larger than its own timer value. The position distribution of all nodes meeting one of the two conditions follows a Matérn CSMA point process [23], which is denoted by Φ_c.

IV. Uplink Local Delay Model

In this section, we derive an analytical model for analyzing the uplink local delay in the network scenario shown in Fig. 1.

According to the definition of the local delay in Section I, the uplink local delay is defined as the time taken for a vehicle node to successfully transmit a packet over the link to the corresponding edge node. According to assumption (5) in Section III.B, each node can transmit a packet only in a timeslot. To transmit a packet in a timeslot, a node will contend for the channel via CSMA. After succeeding in channel contention, it will transmit the packet onto the link. If there is no neighbor in the contention domain of the node or the node has the minimum timer value among all neighbors in its contention domain, the packet will be successfully transmitted onto the link. Otherwise, the transmission of the packet will fail. In this case, the vehicle node needs to retransmit the packet in another timeslot, causing one additional slot delay. If the packet is successfully transmitted onto the link and the SIR at the receiving node is beyond a certain threshold, the packet can be successfully received. Otherwise, the transmission of the packet will also fail. In this case, the vehicle node also needs to retransmit the packet, causing one additional slot delay as well. Therefore, the uplink local delay depends on the number of retransmissions of a packet over a link. Since a retransmission over a link can be caused either by an unsuccessful channel access of a transmitting node or by a small SIR at a receiving node, we need first to analyze the successful channel access probability of a transmitting node and the probability that the SIR at a receiving node is beyond a certain threshold.

A. Successful Access Probability

The successful access probability is defined as the probability that a transmitting node on lane *i* ($i = 0, 1, \ldots, N$) successfully transmits a packet onto a link in a timeslot.

Let $N_{neighbor}$, $N_{neighbor}^{e}$, and $N_{neighbor}^{v_j}$ denote the overall number of neighbors of a node, the number of edge node neighbors of a node, and the number of vehicle node neighbors on lane *j* of a node, respectively. Obviously, we have

$$N_{neighbor} = N_{neighbor}^{e} + \sum_{j=1}^{N} N_{neighbor}^{v_j}. \tag{1}$$

Thus, the average number of neighbors for a particular node is given by

$$E\left[N_{neighbor}\right] = E\left[N_{neighbor}^{e}\right] + \sum_{j=1}^{N} E\left[N_{neighbor}^{v_j}\right]. \tag{2}$$

and $E[N_{neighbor}^{e}]$ and $E[N_{neighbor}^{v_j}]$ are, respectively, given by

$$\begin{aligned} E\left[N_{neighbor}^{e}\right] &= E^{0}\left[\sum_{x \in \Phi_e} \mathbf{1}\left(h_{x,o} d_{x,o}^{-\alpha} P_e \geq P_d\right)\right] \\ &= \lambda_e \int_{\mathcal{R}^2} P\left\{h_{x,o} \geq \frac{P_d}{P_e} d_{x,o}^{\alpha}\right\} d\|x\| \\ &= \lambda_e \int_{[1-\delta(i)]d+(i-1)u(i-1)l}^{\sqrt{L^2+\{[1-\delta(i)]d+(i-1)u(i-1)l\}^2}} e^{-\frac{P_d}{P_e}\cdot\|x\|^{\alpha}} d\|x\|, \end{aligned} \tag{3}$$

$$E\left[N_{neighbor}^{v_j}\right] = E^0\left[\sum_{x\in\Phi_v^i\setminus\{x_0\}} \mathbf{1}\left(h_{x,o}d_{x,o}^{-\alpha}P_v \geq P_d\right)\right]$$
$$= \lambda_v^j \int_{\mathcal{R}^2} P\left\{h_{x,o} \geq \frac{P_d}{P_v}d_{x,o}^{\alpha}\right\} d\|x\|$$
$$= \lambda_v^j \int_{|i-j|l+\delta(j)(d-l)}^{\sqrt{L^2+[|i-j|l+\delta(j)(d-l)]^2}} e^{-\frac{P_d}{P_v}\cdot\|x\|^{\alpha}} d\|x\|, \quad (4)$$

where $\mathcal{R}^2$ is a 2-D real number domain, $E^0[\bullet]$ represents a Palm distribution [25], P_d represents the detection power threshold at a node, P_e represents the transmitting power of an edge node, P_v represents the transmitting power of a vehicle node, $\delta(\bullet)$ is the unit impulse sequence function, and $u(\bullet)$ is the unit step sequence function.

Let p_A^i denote the probability that a node on lane i ($i = 0, 1, \ldots, N$) successfully accesses a channel in a timeslot and t_x denote the timer value of node x. According to the discussion in Section III.B, a node x must meet one of the two conditions to successfully access a channel. Thus, according to [23], we have

$$p_A^i = E^0\left[\mathbf{1}\left(N_{neighbor}=0\right)\|\mathbf{1}\left(t_x < t_y\right), y \in \Phi_{\text{neighbor}}\right], \quad (5)$$

where node y is a neighbor of node x. $\Phi_{neighbor}$ is a set of positions of the neighbors in the contention domain of a node. According to Slivnyak's Theorem [23], we can obtain

$$p_A^i = \frac{1 - e^{-\left\{\sum_{j=1}^{N} E\left[N_{neighbor}^{v_j}\right] + E\left[N_{neighbor}^{e}\right]\right\}}}{\sum_{j=1}^{N} E\left[N_{neighbor}^{v_j}\right] + E\left[N_{neighbor}^{e}\right]}. \quad (6)$$

For the detailed derivation of Eq. (6), readers are referred to [23].

B. Successful Receiving Probability

The successful receiving probability is defined as the probability that a packet transmitted by a service requesting vehicle node on lane i ($i = 1, 2, \ldots, N$) onto a link in a timeslot is successfully received at the serving edge node.

As discussed earlier, the receiving probability depends on the SIR at the serving edge node. Thus, we first analyze the interferences at the serving edge node. We consider a service requesting vehicle node x_0 on lane i, and assume that the position of the serving edge node is an origin, which is denoted by o, as shown in Fig. 2. Since it is assumed that both the spatial distributions of the vehicle nodes and edge nodes in the network are stationary, the origin can be extended to the position of any serving edge node in the network.

Let I_e denote the interference from all interferers at the serving edge node, which can be expressed as

$$I_e = I_e^{\text{edge}} + I_e^{veh}, \quad (7)$$

where I_e^{edge} represents the interference from other edge nodes, and I_e^{veh} represents the interference from all vehicle nodes except the corresponding service requesting node. Meanwhile, let ζ denote an indicator that indicates the transmission state of a node. It is a Boolean variable and is defined as

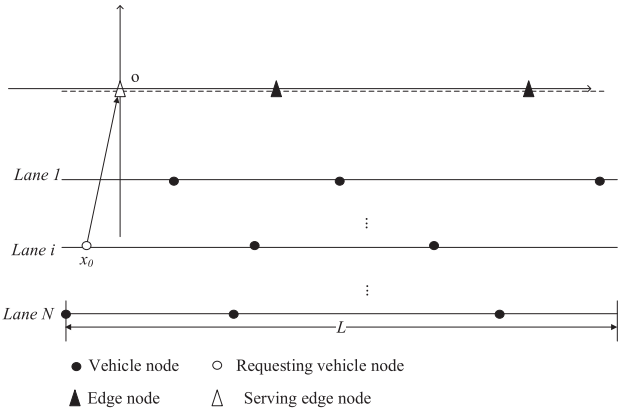

Fig. 2. Illustration of the positions of a requesting vehicle node and the serving edge node.

$$\zeta = \mathbf{1}\left(x \in \Phi_c : x \in \Phi_e \cup \Phi_v\right). \quad (8)$$

When the location of a node x belongs to Φ_c, the value of ζ is 1. Otherwise, the value of ζ is 0. Obviously, $I_e^{edge}$and I_e^{veh} can be expressed as

$$I_e^{\text{edge}} = \sum_{x\in\Phi_e} \zeta \cdot h_{x,o}d_{x,o}^{-\alpha}P_e, \quad (9)$$

$$I_e^{veh} = \sum_{i=1}^{N} \sum_{x_i\in\Phi_v^i\setminus\{x_0\}} \zeta \cdot h_{x_i,o}d_{x_i,o}^{-\alpha}P_v, \quad (10)$$

where x_0 is the position of the service requesting vehicle node, x is the position of an edge node interferer, and x_i is the position of a vehicle node interferer on lane i. Thus, the signal-to-interference ratio (SIR) at the serving edge node is given by

$$SIR = \frac{h_{x_0,o}||x_0||^{-\alpha}P_v}{I_e}. \quad (11)$$

To obtain the successful receiving probability, we perform the Laplace transform of the interference. Obviously, we have

$$\mathcal{L}_{I_e}(s) = \mathcal{L}_{I_e^{edge}+I_e^{veh}}(s) = \mathcal{L}_{I_e^{edge}}(s)\mathcal{L}_{I_e^{veh}}(s). \quad (12)$$

According to Eq. (9)–Eq. (12), the Laplace transform of the interference depends on the distribution of the distance between an interferer (either an edge node or a vehicle node) and the origin, and the distribution of the distance between the service requesting vehicle node and the origin. Since CSMA is employed as the channel access mechanism, either the edge nodes retained by CSMA or the vehicle nodes on lane i ($i = 1, 2, \ldots, N$) retained by CSMA cannot form a PPP. Both the distribution function of the distance between two retained edge nodes and that of the distance between two retained vehicle nodes on lane i ($i = 1, 2, \ldots, N$) cannot be expressed in a closed form. Thus, the Laplace transform of the interference cannot be expressed in a closed form either. These make it difficult to analyze the local delay mathematically. To address this problem, it is necessary to reasonably approximate the Laplace transform of the interference into a closed form, which is the major challenge in deriving the successful receiving probability.

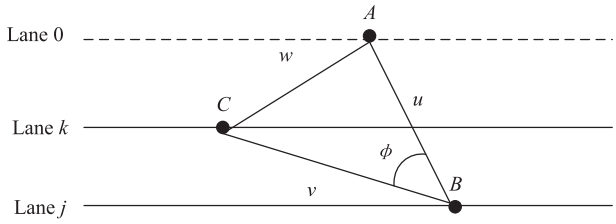

Fig. 3. Illustration of node positions (1).

To approximate the Laplace transform of the interference for the serving edge node, we use the interference from a PPP with density $\lambda_v^i h_v^i(u)$ and the interference from a PPP with density $\lambda_e h_e(u)$ to approximate the interference from other vehicle nodes and the interference from other edge nodes [23], respectively. Here, $h_e(u)$ denotes the probability that node A ($A \in \Phi_e$) successfully accesses the channel under the condition that node B ($B \in \Phi_v^j (j = 1, 2, \ldots, N)$) already successfully accesses the channel when the distance between node A and node B is u. $h_v^i(u)$ denotes the probability that node A ($A \in \Phi_v^i, i = 1, 2, \ldots, N$) successfully accesses the channel under the condition that node B ($B \in \Phi_v^j (j = 1, 2, \ldots, N)$) already successfully accesses the channel when the distance between node A and node B is u. Next we analyze $h_e(u)$ and $h_v^i(u)$, respectively.

1) *Analysis of* $h_e(u)$*:* For analysis of $h_e(u)$, we consider node A, node B, and node C as shown in Fig. 3, where node A is an edge node on lane 0 (i.e., $A \in \Phi_e$), node B is a vehicle node on lane j (i.e., $B \in \Phi_v^j$, $j = 1, 2, \ldots, N$), and node C is any node on lane k (i.e., $C \in \Phi_e \cup \Phi_v^k$, $k = 1, 2, \ldots, N$). The distance between node A and node B is denoted by u. The distance between node B and node C is denoted by v. The distance between node A and node C is denoted by w.

Assume that the timer value of edge node B is larger than the timer value of node A, i.e., $t_B > t_A$. According to [23] and [26], $h_e(u)$ is given by

$$h_e(u) = \int_{t_A, t_B} \frac{P_e^1}{P_e^2} dt_A dt_B, \tag{13}$$

where P_e^1 is the probability that neither node A nor node B detects any node in $\Phi^{t_A} = \{x \in \Phi_v \cup \Phi_e : t_x < t_A\}$, and P_e^2 is the reciprocal of the probability that node B does not detect any node in $\Phi^{(t_A, t_B)} = \{x \in \Phi_v \cup \Phi_e : t_A \le t_x < t_B\}$, including node A.

According to [23], P_e^1 can be obtained by using the Poisson distribution of the number of nodes, which are in Φ^{t_A}, and are detected by both node A and node B. Thus, we have

$$P_e^1 = e^{-\lambda_e t_A \int R_1(v) dv} \cdot \prod_{k=1}^{N} e^{-\lambda_v^k t_A \int R_2(v) dv}, \tag{14}$$

where $R_1(v)$ denotes the probability that both node A and node B detect node C belonging to Φ_e, and is given by

$$\begin{aligned} &R_1(v) \\ &= 1 - P\left\{h_{A,C} \cdot \|A - C\|^{-\alpha} P_e < P_d\right\} \\ &\quad \cdot P\left\{h_{B,C} \cdot \|B - C\|^{-\alpha} P_e < P_d\right\} \\ &= 1 - \left(1 - e^{-\frac{P_d}{P_e}\|A-C\|^{\alpha}}\right)\left(1 - e^{-\frac{P_d}{P_e}\|B-C\|^{\alpha}}\right) \\ &= e^{-\frac{P_d}{P_e} w^{\alpha}} + e^{-\frac{P_d}{P_e} v^{\alpha}} - e^{-\frac{P_d}{P_e} w^{\alpha}} e^{-\frac{P_d}{P_e} v^{\alpha}} \end{aligned} \tag{15}$$

and $R_2(v)$ denotes the probability that both node A and node B detect node C belonging to $\Phi_v^k (k = 1, 2, \ldots, N)$, which is given by

$$\begin{aligned} &R_2(v) \\ &= 1 - P\left\{h_{A,C} \cdot \|A - C\|^{-\alpha} P_v < P_d\right\} \\ &\quad \cdot P\left\{h_{B,C} \cdot \|B - C\|^{-\alpha} P_v < P_d\right\} \\ &= 1 - \left(1 - e^{-\frac{P_d}{P_v}\|A-C\|^{\alpha}}\right)\left(1 - e^{-\frac{P_d}{P_v}\|B-C\|^{\alpha}}\right). \\ &= e^{-\frac{P_d}{P_v} w^{\alpha}} + e^{-\frac{P_d}{P_v} v^{\alpha}} - e^{-\frac{P_d}{P_v} w^{\alpha}} e^{-\frac{P_d}{P_v} v^{\alpha}} \end{aligned} \tag{16}$$

For ease of further analysis, we use polar coordinates to describe the position relationship between node A, node B, and node C in Eq. (15) and Eq. (16). Specifically, we assume that the position of node B is an origin, the angle between $\vec{BC}$ and $\vec{BA}$ is ϕ, as shown in Fig. 3. Thus, $R_1(v)$ and $R_2(v)$ can be written as

$$\begin{aligned} R_1(v) &= e^{-\frac{P_d}{P_e} v^{\alpha}} + e^{-\frac{P_d}{P_e}\left(\sqrt{u^2+v^2-2uv\cos\phi}\right)^{\alpha}} \\ &\quad - e^{-\frac{P_d}{P_e}\left[\left(\sqrt{u^2+v^2-2uv\cos\phi}\right)^{\alpha} + v^{\alpha}\right]} \\ &\triangleq f_1(u, v, \phi) \end{aligned} \tag{17}$$

$$\begin{aligned} R_2(v) &= e^{-\frac{P_d}{P_v} v^{\alpha}} + e^{-\frac{P_d}{P_v}\left(\sqrt{u^2+v^2-2uv\cos\phi}\right)^{\alpha}} \\ &\quad - e^{-\frac{P_d}{P_v}\left[\left(\sqrt{u^2+v^2-2uv\cos\phi}\right)^{\alpha} + v^{\alpha}\right]} \\ &\triangleq f_2(u, v, \phi). \end{aligned} \tag{18}$$

$$\int R_2(v) dv = \begin{cases} \int_{\arctan\frac{(j-1)l+d}{L}}^{\pi} + \arctan\frac{(k-j)l+d}{L} \int_{(k-j)l}^{\sqrt{L^2+[(k-j)l]^2}} f_2(u, v, \phi) v dv d\phi, & j < k \\ \frac{1}{2}\left\{\int_{\frac{\pi}{2}}^{\pi - \arctan\frac{(k-1)l+d}{L}} \int_0^L f_2(u, v, \phi) v dv d\phi + \int_{\arctan\frac{(k-1)l+d}{L}}^{\frac{\pi}{2}} \int_0^L f_2(u, v, \phi) v dv d\phi\right\}, & j = k \\ \int_0^{\arctan\frac{\sqrt{\tau_1{}^2 - [(j-k)l]^2}}{(j-k)l} + \arctan\frac{L - \sqrt{\tau_1{}^2 - [(j-k)l]^2}}{(j-1)l+d}} \int_{(j-k)l}^{\sqrt{L^2+[(j-k)l]^2}} f_2(u, v, \phi) v dv d\phi, & j > k \end{cases} \tag{20}$$

By using the spatial distributions of node *A*, node *B*, and node *C*, we have

$$\int R_1(v)dv = \int_0^{\pi-2\arctan\frac{2[(j-1)l+d]}{L}} \times \int_{(j-1)l+d}^{\sqrt{L^2+[(j-1)l+d]^2}} f_1(u,v,\phi)\, v dv d\phi \quad (19)$$

and eq. (20) shown at the bottom of the previous page, where

$$\tau_1 = (j-k)\, l\sqrt{1+\left[\frac{L}{(j-k)\, l+(j-1)\, l+d}\right]}. \quad (21)$$

Similar to P_e^1, P_e^2 can be obtained by using the Poisson distribution of the number of nodes, which are in $\Phi^{(t_A,t_B)}$, and are detected by both node *A* and node *B*. Thus, we have

$$P_e^2 = P\left\{h_{A,B}\cdot u^{-\alpha}P_v < P_d\right\}\cdot e^{-\lambda_e(t_B-t_A)\int Q_1(v)dv} \cdot \prod_{k=1}^{N} e^{-\lambda_v^k(t_B-t_A)\int Q_2(v)dv}, \quad (22)$$

where $Q_1(v)$ is the probability that node *B* detects node *C* ($C\in\Phi_e$), which is given by

$$Q_1(v) = 1 - P\left\{h_{B,C}\cdot v^{-\alpha}P_e < P_d\right\}, \quad (23)$$

and $Q_2(v)$ is the probability that node *B* detects node *C* ($C\in\Phi_v^k, k=1,2,\ldots,N$), which is given by

$$Q_2(v) = 1 - P\left\{h_{B,C}\cdot v^{-\alpha}P_v < P_d\right\}. \quad (24)$$

Thus, we have

$$\int Q_1(v)\, dv = \int_{(j-1)l+d}^{\sqrt{L^2+[(j-1)l+d]^2}} e^{-\frac{P_d}{P_e}v^\alpha} dv \quad (25)$$

and

$$\int Q_2(v)\, dv = \int_{|k-j|l}^{\sqrt{L^2+[|k-j|l]^2}} e^{-\frac{P_d}{P_v}v^\alpha} dv. \quad (26)$$

By substituting Eq. (19)–Eq. (21) into Eq. (14) and substituting Eq. (25) and Eq. (26) into Eq. (22), we can obtain P_e^1 and P_e^2, respectively. By substituting P_e^1 and P_e^2, and de-conditioning with respect to t_A and t_B, we can obtain $h_e(u)$.

2) *Analysis of* $h_v^i(u)$*:* According to [26], $h_v^i(u)$ is given by

$$h_v^i(u) = \int_{t_A,t_B} \frac{P_{v_i}^1}{P_{v_2}^2} dt_A dt_B, \quad (27)$$

where $P_{v_i}^1$ is the probability that neither node *A* ($A\in\Phi_v^i,\ i=1,2,\ldots,N$) nor node *B* ($B\in\Phi_v^j,\ j=1,2,\ldots,N$) detects any node in $\Phi^{t_A}=\{x\in\Phi_v\cup\Phi_e : t_x<t_A\}$, and $P_{v_i}^2$ is the reciprocal of the probability that node *B* does not detect any node in $\Phi^{(t_A,t_B)}=\{x\in\Phi_v\cup\Phi_e : t_A\le t_x<t_B\}$, including node *A*.

According to [26], $P_{v_i}^1$ can be obtained by using the Poisson distribution of the number of nodes, which are in Φ^{t_A}, and are detected by both node *A* and node *B*. Thus, we have

$$P_{v_i}^1 = e^{-\lambda_e t_A\int G_1(v)dv}\cdot\prod_{k=1}^{N} e^{-\lambda_v^k t_A\int G_2(v)dv}, \quad (28)$$

where $G_1(v)$ is the probability that both node *A* and node *B* detect node *C* belonging to Φ_e, which is given by

$$\begin{aligned} G_1(v) &= 1 - P\left\{h_{A,C}\cdot\|A-C\|^{-\alpha}P_e < P_d\right\} \\ &\quad\cdot P\left\{h_{B,C}\cdot\|B-C\|^{-\alpha}P_e < P_d\right\} \\ &= 1-\left(1-e^{-\frac{P_d}{P_e}\|A-C\|^\alpha}\right)\left(1-e^{-\frac{P_d}{P_e}\|B-C\|^\alpha}\right) \\ &= e^{-\frac{P_d}{P_e}w^\alpha}+e^{-\frac{P_d}{P_e}v^\alpha}-e^{-\frac{P_d}{P_e}w^\alpha}e^{-\frac{P_d}{P_e}v^\alpha} \end{aligned} \quad (29)$$

and $G_2(v)$ is the probability that both node *A* and node *B* detect node *C* belonging to $\Phi_v^k (k=1,2,\ldots,N)$, which is given by

$$\begin{aligned} G_2(v) &= 1 - P\left\{h_{A,C}\cdot\|A-C\|^{-\alpha}P_v < P_d\right\} \\ &\quad\cdot P\left\{h_{B,C}\cdot\|B-C\|^{-\alpha}P_v < P_d\right\} \\ &= 1-\left(1-e^{-\frac{P_d}{P_v}\|A-C\|^\alpha}\right)\left(1-e^{-\frac{P_d}{P_v}\|B-C\|^\alpha}\right) \\ &= e^{-\frac{P_d}{P_v}w^\alpha}+e^{-\frac{P_d}{P_v}v^\alpha}-e^{-\frac{P_d}{P_v}w^\alpha}e^{-\frac{P_d}{P_v}v^\alpha} \end{aligned} \quad (30)$$

Note that in the above analyses, Eq. (29) and Eq. (15) have the same form, and Eq. (30) and Eq. (16) have the same form. The only difference between them is whether node *A* belongs to Φ_e or $\Phi_v^i (i=1,2,\ldots,N)$.

By using polar coordinates and the spatial distributions of node *A*, node *B*, and node *C*, we have Eq. (31) shown at the bottom of this page

$$\tau_2 = [(j-1)\, l+d]\cdot\sqrt{1+\left\{\frac{L}{[(j-1)\, l+d]+[(j-i)\, l]}\right\}^2}, \quad (32)$$

$$\int G_1(v)dv = \begin{cases} \int_{\arctan\frac{(j-1)l+d}{L}+\arctan\frac{(i-j)l+d}{L}}^{\pi}\int_{(j-1)l+d}^{\sqrt{L^2+[(j-1)l+d]^2}} f_1(u,v,\phi)vdvd\phi, & j<i \\ \frac{1}{2}\left\{\int_{\frac{\pi}{2}}^{\pi-\arctan\frac{(j-1)l+d}{L}}\int_{(j-1)l+d}^{\sqrt{L^2+[(j-1)l+d]^2}} f_1(u,v,\phi)vdvd\phi\right. \\ \quad\left.+\int_{\arctan\frac{(j-1)l+d}{L}}^{\frac{\pi}{2}}\int_{(j-1)l+d}^{\sqrt{L^2+[(j-1)l+d]^2}} f_1(u,v,\phi)vdvd\phi\right\}, & j=i \\ \int_0^{\arctan\frac{\sqrt{{\tau_2}^2-[(j-1)l+d]^2}}{(j-1)l+d}+\arctan\frac{L-\sqrt{{\tau_2}^2-[(j-1)l+d]^2}}{(j-i)l}}\int_{(j-1)l+d}^{\sqrt{L^2+[(j-1)l+d]^2}} f_1(u,v,\phi)vdvd\phi, & j>i \end{cases} \quad (31)$$

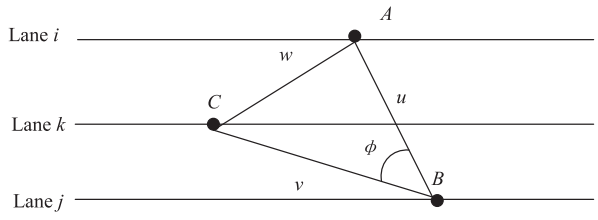

Fig. 4. Illustration of node positions (2).

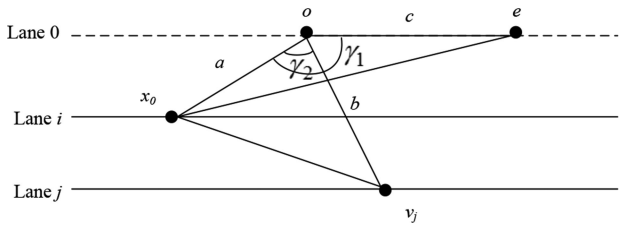

Fig. 5. Illustration of node positions (3).

and

$$\int G_2(v)\,dv = \begin{cases} \int_0^{\arctan\frac{\sqrt{{\tau_3}^2-[(k-j)l]^2}}{|k-j|l}+\arctan\frac{L-\sqrt{{\tau_3}^2-[(k-j)l]^2}}{|j-i|l}} \int_{|k-j|l}^{\sqrt{L^2+[|k-j|l]^2}} f_2(u,v,\phi)\,vdvd\phi, \\ j>k\geq i;\ \ j>i>k;\ \ j<i=k \\ \int_{\arctan\frac{|j-i|l}{L}+\arctan\frac{|j-k|l}{L}}^{\pi} \int_{|j-k|l}^{\sqrt{L^2+[|j-k|l]^2}} f_2(u,v,\phi)\,vdvd\phi,\ k>j>i; i>j>k \\ \int_{\arctan\frac{|i-k|l}{L}}^{\pi-\arctan\frac{|i-k|l}{L}} \int_{|i-k|l}^{\sqrt{L^2+[|i-k|l]^2}} f_2(u,v,\phi)\,vdvd\phi,\ j=i>k; \\ j=i<k; j=k<i; k=j>i \\ \frac{2}{3}\int_0^L \left[e^{-\frac{P_d}{P_v}v^\alpha}+e^{-\frac{P_d}{P_v}|u-v|^\alpha}-e^{-\frac{P_d}{P_v}(v^\alpha+|u-v|^\alpha)}\right] \\ d\tau+\frac{1}{3}\int_0^L \left[e^{-\frac{P_d}{P_v}v^\alpha}+e^{-\frac{P_d}{P_v}(u+v)^\alpha}\right. \\ \left.-e^{-\frac{P_d}{P_v}(v^\alpha+(u+v)^\alpha)}\right],\ i=j=k \end{cases} \tag{33}$$

$$\tau_3 = |k-j|\,l\cdot\sqrt{1+\left\{\frac{L}{|k-j|\,l+|j-i|\,l}\right\}^2}. \tag{34}$$

Fig. 4 shows the position relationship between node *A*, node *B*, and node *C*, where $A\in\Phi_v^i (i=1,2,\ldots,N)$, $B\in\Phi_v^j$ $(j=1,2,\ldots,N)$, and $C\in\Phi_e\cup\Phi_v^k$ $(k=1,2,\ldots,N)$.

Similar to $P_{v_i}^1$, $P_{v_i}^2$ can be obtained by the Poisson distribution of the number of nodes, which are in $\Phi^{(t_A,t_B)}$, and are detected by both node *A* and node *B*. Thus, we have

$$P_{v_i}^2 = P\left\{h_{A,B}\cdot u^{-\alpha}P_v < P_d\right\}\cdot e^{-\lambda_e(t_B-t_A)\int Q_1(v)dv} \cdot\prod_{k=1}^{N} e^{-\lambda_v^k(t_B-t_A)\int Q_2(v)dv}. \tag{35}$$

By substituting Eq. (31)–Eq. (34) into Eq. (28) and substituting Eq. (25) and Eq. (26) into Eq. (35), we can obtain $P_{v_i}^1$ and $P_{v_i}^2$, respectively. By substituting $P_{v_i}^1$ and $P_{v_i}^2$, and de-conditioning with respect to t_A and t_B, we can obtain $h_v^i(u)$.

With $h_e(u)$ and $h_v^i(u)$, the Laplace transform of the interferences I_e^{edge} and I_e^{veh} can be obtained by using the Poisson approximation [23], i.e.,

$$\mathcal{L}_{I_e^{edge}}(s) = E\left[\exp\left(-sI_e^{edge}\right)\right] = E\left[\exp\left(-s\sum_{x\in\Phi_e}\zeta\cdot h_{x,o}d_{x,o}^{-\alpha}P_e\right)\right]$$
$$= E\left[\prod_{x\in\Phi_e}\exp\left(-s\zeta\cdot h_{x,o}d_{x,o}^{-\alpha}P_e\right)\right]$$
$$\overset{(a)}{=} E_{\Phi_e}\left[\prod_{x\in\Phi_e}\left(\frac{1}{1+s\zeta d_{x,o}^{-\alpha}P_e}\right)\right]$$
$$\overset{(b)}{=} E\left[\exp\left(-\lambda_e\int_{\mathcal{R}^2}\frac{h_e\left(d_{x0,e}\right)sd_{x,o}^{-\alpha}P_e}{1+sd_{x,o}^{-\alpha}P_e}d\left\|x\right\|\right)\right], \tag{36}$$

$$\mathcal{L}_{I_e^{veh}}(s) = E\left[\exp\left(-sI_e^{veh}\right)\right] = E\left[\exp\left(-s\sum_{j=1}^{N}\sum_{x_j\in\Phi_v^j\setminus\{x_0\}}\zeta\cdot h_{x_j,o}d_{x_j,o}^{-\alpha}P_v\right)\right]$$
$$= \prod_{j=1}^{N}E\left[\prod_{x_j\in\Phi_v^j\setminus\{x_0\}}\exp\left(-s\zeta\cdot h_{x_j,o}d_{x_j,o}^{-\alpha}P_v\right)\right]$$
$$\overset{(a)}{=}\prod_{j=1}^{N}E_{\Phi_v^j}\left[\prod_{x_j\in\Phi_v^j\setminus\{x_0\}}\left(\frac{1}{1+s\zeta d_{x_j,o}^{-\alpha}P_v}\right)\right]$$
$$\overset{(b)}{=} E\left[\prod_{j=1}^{N}\exp\left(-\lambda_v^j\int_{\mathcal{R}^2}\frac{h_v^j\left(d_{x_0,v_j}\right)sd_{x_j,o}^{-\alpha}P_v}{1+sd_{x_j,o}^{-\alpha}P_v}d\left\|x_j\right\|\right)\right] \tag{37}$$

where (a) follows from the fact that the distribution of $h_{x,y}$ is an independent exponential distribution with mean 1 and (b) follows from the probability generating functional (PGFL) [25].

Next we derive the successful receiving probability at the serving edge node based on the above results. Fig. 5 illustrates the position relationship between a requesting vehicle node (x_0), the serving edge node (o), an edge node interferer (e), and a vehicle node interferer on lane j (v_j).

In Fig. 5, a denotes the distance between the requesting vehicle node and the origin, b denotes the distance between a vehicle node interferer on lane j and the origin, c denotes the distance between an edge node interferer and the origin, γ_1 denotes the angle between $\vec{oe}$ and $\vec{ox_0}$, and γ_2 denotes the angle between $\vec{ov_j}$ and $\vec{ox_0}$.

According to the definition of the successful receiving probability, we have

$$p_R^i = P\left\{SIR>\theta\right\}, \tag{38}$$

where θ is the SIR threshold at the serving edge node. According to Eqs. (11)–(14), we have Eqs. (39) and (40) shown at the bottom of the next page.

For ease of exposition, we use polar coordinates to describe the position relationship between the service requesting vehicle node, the serving edge node, the edge node interferer, and the vehicle node interferer. Meanwhile, we use a, b, c to represent the corresponding distances instead of $d_{x_0,o}$, $d_{v_j,o}$ and $d_{e,o}$, respectively.

According to [27], by using the distribution of a, b, and c, p_R^i can further be written as Eq. (40), where

$$g(a) = \frac{a\lambda_e\left(1-p_A^0\right)}{\sqrt{a^2-\left[(i-1)\,l+d\right]^2}} \cdot e^{-\lambda_e\left(1-p_A^0\right)\sqrt{a^2-\left[(i-1)l+d\right]^2}}, \tag{41}$$

$$\tau_4 = \left[(j-1)\,l+d\right]\sqrt{1+\left\{\frac{L}{\left[(j-1)\,l+d\right]+\left[(i-1)\,l+d\right]}\right\}^2}, \tag{42}$$

$$d_{x_0,e} = \sqrt{a^2+c^2-2ac\cos\gamma_1}, \tag{43}$$

$$d_{x_0,v_j} = \sqrt{a^2+b^2-2ab\cos\gamma_2}. \tag{44}$$

$$\omega = \arctan\frac{\sqrt{{\tau_4}^2-\left[(j-1)\,l+d\right]^2}}{(j-1)\,l+d} + \arctan\frac{L-\sqrt{{\tau_4}^2-\left[(j-1)\,l+d\right]^2}}{(i-1)\,l+d} \tag{45}$$

C. Uplink Local Delay

As defined earlier, the uplink local delay is the time taken for a vehicle node to successfully transmit a packet over the link to its serving edge node, which depends on the number of retransmissions of a packet over the link. Since it takes one timeslot for each packet retransmission over the link, it is necessary to know the probability that a packet is successfully transmitted over the link in one timeslot in order to obtain the uplink local delay.

Let p_T^i denote the probability that a packet sent by a service requesting vehicle node on lane i is successfully transmitted over a link in one timeslot. According to the analysis in Section IV, p_T^i depends on the successful access probability of the requesting vehicle node and the probability that the SIR at the serving edge node is beyond a certain threshold. Thus, we have

$$p_T^i = p_A^i p_R^i. \tag{46}$$

Therefore, the uplink local delay for a service requesting vehicle node on lane i is given by

$$D_i = \frac{1}{p_T^i}, \quad i = 1, 2, \ldots, N. \tag{47}$$

V. Numerical Results

In this section, we validate the derived uplink local delay model through simulation results and analyze the uplink local delay under major parameters. We conducted a Monte Carlo simulation experiment using Matlab. In the experiment, we set $N = 2$ and $L = 2$ km. Without loss of generality, we consider the uplink local delay of a requesting vehicle node on lane 1. Moreover, we generate three independent PPPs: the PPP of edge nodes, the PPP of vehicles on lane 1, and the PPP of vehicles on lane 2. The other parameters were set according to [18] and [24], namely, $l = d = 4$ m, $P_d = -78$ dBm, $P_e = 13$ dBm, and $P_v = 10$ dBm. The experiment was repeated over 1000 times and each result is an average over 1000 repetitions.

Fig. 6–Fig. 11 show the simulation results obtained through the simulation experiments and the numerical results obtained using the derived analytical model. It is seen that the simulation

$$\begin{aligned} p_R^i &= P\left\{\frac{h_{x_0,o}d_{x_0,o}^{-\alpha}P_v}{I_e} > \theta\right\} = P\left\{h_{x_0,o} > \frac{\theta d_{x_0,o}^{\alpha}}{P_v}I_e\right\} = \int_{i_e} P\left\{h_{x_0,o} > \frac{\theta d_{x_0,o}^{\alpha}}{P_v}i_e | I_e = i_e\right\} P_{I_e}(i_e)\, di_e \\ &= \mathcal{L}_{I_e}\left(\frac{\theta d_{x_0,o}^{\alpha}}{P_v}\right) = \mathcal{L}_{I_e^{edge}+I_e^{veh}}\left(\frac{\theta d_{x_0,o}^{\alpha}}{P_v}\right) = \mathcal{L}_{I_e^{edge}}\left(\frac{\theta d_{x_0,o}^{\alpha}}{P_v}\right)\mathcal{L}_{I_e^{veh}}\left(\frac{\theta d_{x_0,o}^{\alpha}}{P_v}\right) \\ &= E\left[\exp\left(-\lambda_e\int_{\mathcal{R}^2}\frac{h_e(d_{x_0,e})\,\frac{\theta d_{x_0,o}^{\alpha}}{P_v}P_e d_{x,o}^{-\alpha}}{1+\frac{\theta d_{x_0,o}^{\alpha}}{P_v}P_e d_{x,o}^{-\alpha}} d\|x\|\right)\right] \cdot E\left[\prod_{j=1}^{N}\exp\left(-\lambda_v^j\int_{\mathcal{R}^2}\frac{h_v^j(d_{x_0,v_j})\,\theta d_{x_0,o}^{\alpha}d_{x_j,o}^{-\alpha}}{1+\theta d_{x_0,o}^{\alpha}d_{x_j,o}^{-\alpha}} d\|x_j\|\right)\right] \end{aligned} \tag{39}$$

$$\begin{aligned} p_R^i = &\int_{(i-1)l+d}^{\sqrt{L^2+[(i-1)l+d]^2}} \exp\left(-\lambda_e\int_{\arctan\frac{(i-1)l+d}{L}}^{\pi-\arctan\frac{(i-1)l+d}{L}}\int_0^L \frac{h_e(d_{x_0,e})}{1+\frac{P_v}{\theta P_e}\left(\frac{c}{a}\right)^{\alpha}} c\,dc\,d\gamma_1\right) g(a)\,da \\ &\cdot \prod_{j=1,j\neq i}^{N}\int_{(i-1)l+d}^{\sqrt{L^2+[(i-1)l+d]^2}} \exp\left(-\lambda_v^j\int_0^{\omega}\int_{[(j-1)l+d]}^{\sqrt{L^2+[(j-1)l+d]^2}} \frac{h_v^j(d_{x_0,v_j})}{1+\frac{1}{\theta}\left(\frac{b}{a}\right)^{\alpha}}\cdot\frac{b}{\sqrt{b^2-\left[(j-1)\,l+d\right]^2}}\cdot b\,db\,d\gamma_2\right) g(a)\,da \\ &\cdot \int_{(i-1)l+d}^{\sqrt{L^2+[(i-1)l+d]^2}} \exp\left(-\lambda_v^j\int_0^{\pi-2\arctan\frac{(i-1)l+d}{L}}\int_{[(i-1)l+d]}^{\sqrt{L^2+[(i-1)l+d]^2}} \frac{h_v^i(d_{x_0,v_j})}{1+\frac{1}{\theta}\left(\frac{b}{a}\right)^{\alpha}}\cdot\frac{b}{\sqrt{b^2-\left[(i-1)\,l+d\right]^2}}\cdot b\,db\,d\gamma_2\right) g(a)\,da \end{aligned} \tag{40}$$

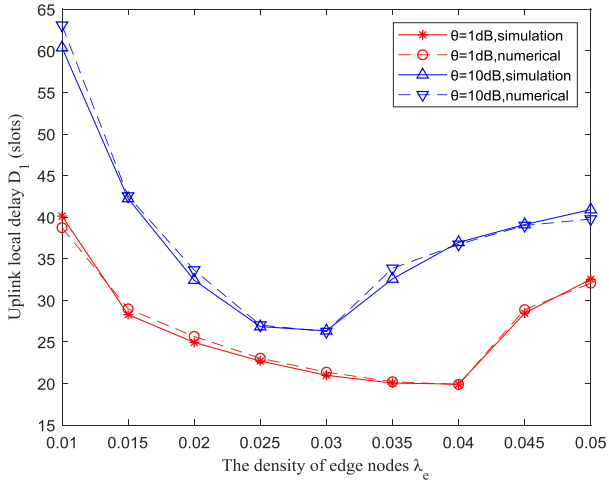

Fig. 6. Uplink local delay D_1 vs the density of edge nodes λ_e ($\alpha = 4, \lambda_v^1 = 0.03, \lambda_v^2 = 0.02$).

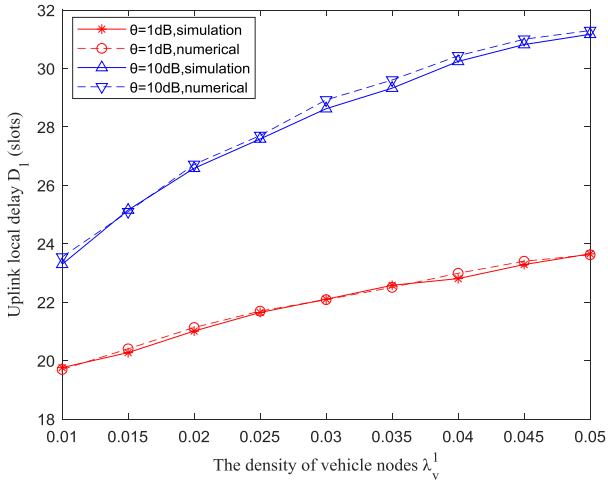

Fig. 7. Uplink local delay D_1 vs the density of vehicle nodes on lane 1 λ_v^1 ($\alpha = 4, \lambda_e = 0.025, \lambda_v^2 = 0.02$).

results are in general close to the numerical results. This demonstrates that the derived analytical model is basically accurate and effective.

Fig. 6 shows the uplink local delay as a function of the density of edge nodes (λ_e) when $\theta = 1$ dB and $\theta = 10$ dB, respectively. It is seen that for a given value of θ, as λ_e increases, the local delay first decreases and then increases. This is because as λ_e initially increases, the average distance between a requesting vehicle node and the corresponding serving edge node becomes smaller, which increases the successful receiving probability of a serving edge node. Meanwhile, as λ_e increases, the channel access probability of a requesting vehicle node decreases due to more edge nodes contending for the channel. But in this case the increase of the successful receiving probability has a larger impact on the local delay than the decrease of the channel access probability, thus causing the local delay to decrease. However, as λ_e continues to increase beyond a certain value, the interference at a serving edge node from other edge nodes has a larger impact on the local delay than the average distance between a requesting vehicle node and the corresponding serving edge node. As a result, the successful receiving probability of a serving edge node decreases, causing the local delay to increase. Thus, there exists an optimal value λ_e^*which minimizes the local delay. Moreover, the optimal value of λ_e with $\theta = 1$ dB is different from that with $\theta = 10$ dB. The larger the value of θ is, the larger the optimal value of λ_e is. This is because a larger value of θ would result in a smaller successful receiving probability and thus a larger local delay. To minimize the local delay, a larger value of λ_e is needed to decrease the average distance between a requesting vehicle node and the corresponding serving edge node and thus increase the successful receiving probability.

Fig. 7 shows the uplink local delay as a function of the density of vehicle nodes on lane 1 (λ_v^1) when $\theta = 1$ dB and $\theta = 10$ dB, respectively. It is seen that the local delay increases with λ_v^1 increasing. This is because as λ_v^1 increases the interference at a serving edge node from vehicle nodes on lane 1 increases as well, which decreases the successful receiving probability of the serving edge node. However, as λ_v^1 increases, the average distance between a requesting vehicle node and the corresponding serving edge node becomes smaller, which increases the successful receiving probability of a serving edge node. Meanwhile, as λ_v^1 increases, the channel access probability of a requesting vehicle node decreases. But the decrease of the channel access probability has a larger impact on the local delay than the increase of the successful receiving probability. As a result, as λ_v^1 increases, the local delay increases.

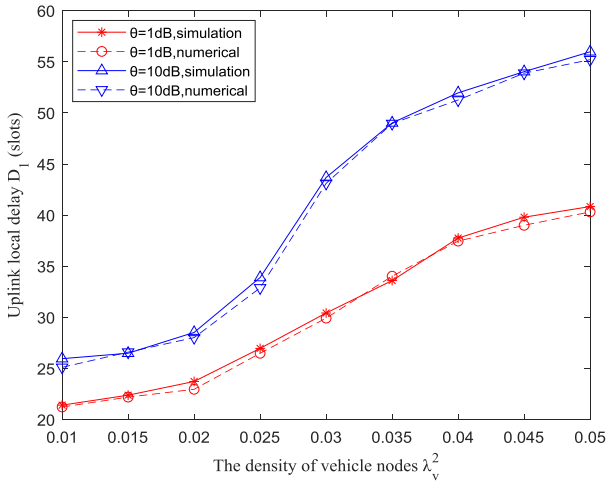

Fig. 8. Uplink local delay D_1 vs the density of vehicle nodes on lane 2 λ_v^2 ($\alpha = 4, \lambda_e = 0.025, \lambda_v^1 = 0.025$).

Fig. 8 shows the uplink local delay as a function of the density of vehicle nodes on lane 2 (λ_v^2) when $\theta = 1$ dB and $\theta = 10$ dB, respectively. It is seen that the local delay increases with λ_v^2 increasing. This is because as λ_v^2 increases the interference at a serving edge node from vehicle nodes on lane 2 increases, which decreases the successful receiving probability of the serving edge node. Moreover, as λ_v^2 increases, the channel access probability of a requesting vehicle node decreases. Both the decrease

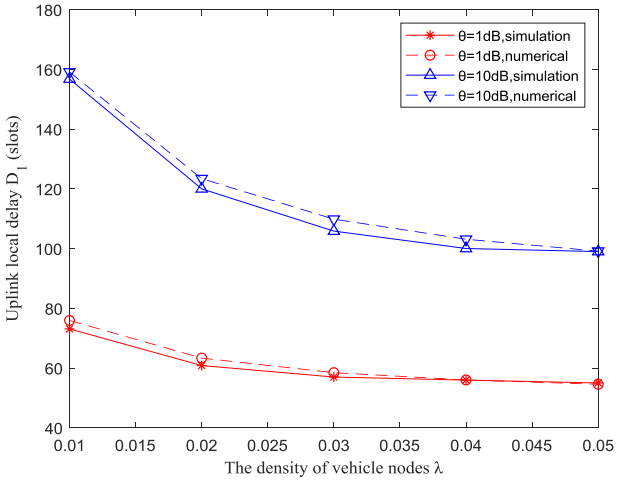

Fig. 9. Uplink local delay D_1 vs the density of vehicle nodes λ ($\alpha = 4, \lambda_e = 0.005, \lambda_v^1 = \lambda_v^2 = \lambda$).

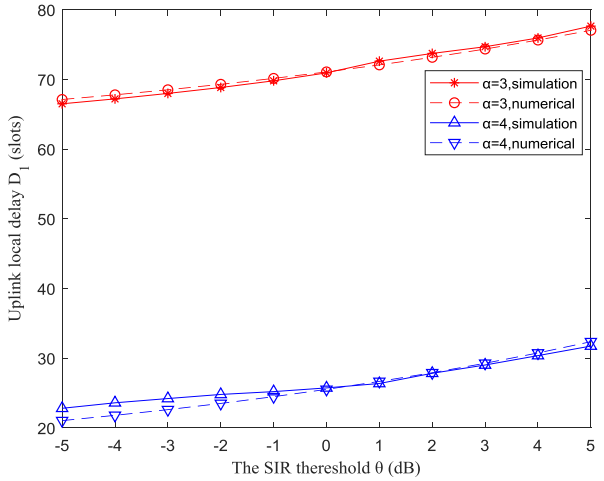

Fig. 10. Uplink local delay D_1 vs the SIR threshold θ ($\lambda_e = 0.01, \lambda_v^1 = 0.04, \lambda_v^2 = 0.025$).

of the successful receiving probability and the decrease of the channel access probability cause the local delay to increase.

Fig. 9 shows the uplink local delay as a function of both the density of vehicles on lane 1 (λ_v^1) and that on lane 2 (λ_v^2) with $\theta = 1$ dB and $\theta = 10$ dB, respectively, when $\lambda_v^1 = \lambda_v^2 = \lambda$. It is seen that for a given value of θ, the local delay gradually decreases with both λ_v^1 and λ_v^2 increasing. This is because as λ_v^1 increases, the average distance between a requesting vehicle node and the corresponding serving edge node becomes smaller, which increases the successful receiving probability of a serving edge node. Meanwhile, as both λ_v^1 and λ_v^2 increase, the interference at a serving edge node from vehicle nodes on both lanes increases as well, which decreases the successful receiving probability of the serving edge node. But in this case the decrease of the average distance between a requesting vehicle node and the corresponding serving edge node has a larger impact on the local delay than the increase of the interference at a serving edge node from vehicle nodes on both lanes. As a result, as both $\lambda_v^1$and λ_v^2 increase, the local delay decreases.

Fig. 10 shows the uplink local delay as a function of the SIR threshold (θ) when $\alpha = 3$ and $\alpha = 4$, respectively. It is seen that for a given value of α, the local delay increases as θ increases. This is because as θ increases the successful receiving probability of a serving edge node decreases, which is obvious. Moreover, a larger value of α results in a smaller value of the local delay. This is because the larger the value of α is, the larger the path loss on the transmission link is, which decreases the interference from other edge nodes and vehicle nodes, and thus increases the successful receiving probability of a serving edge node. As a result, the local delay decreases.

Fig. 11 shows the uplink local delay as a function of the path loss exponent α with $\lambda = 5\lambda_e$ and $\lambda = 10\lambda_e$, respectively, when $\lambda_v^1 = \lambda_v^2 = \lambda$. It is seen that for a given value of λ the local delay increases as αincreases. This is because as α increases the received signal strength at a serving edge node from the corresponding requesting vehicle node decreases, which decreases the successful receiving probability of the serving edge node.

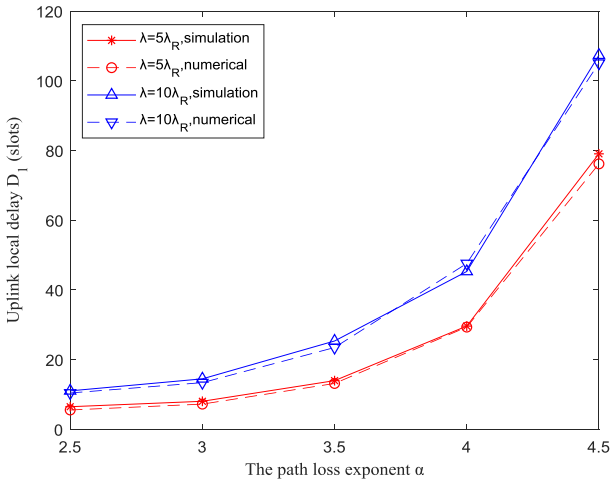

Fig. 11. Uplink local delay D_1 as the path loss exponent α ($\theta = 8$ dB, $\lambda_e = 0.05, \lambda_v^1 = \lambda_v^2 = \lambda$).

As a result, the local delay increases. On the other hand, a larger value of λ results in a larger local delay. This is because the larger the value of $\lambda$is, the more the interference at a serving edge node from vehicles is, which decreases the successful receiving probability of the serving edge node and thus increases the local delay. In addition, as λ increases, the channel access probability of a requesting vehicle node decreases, which increases the local delay as well.

Fig. 12 shows the uplink local delay as a function of the length of each lane (L) when $\alpha = 3$ and $\alpha = 4$, respectively. It is seen that given the value of α, and the values of λ_e, λ_v^1, and λ_v^2, the local delay increases slowly as L increases. This is because in this case as L increases the number of vehicle nodes and edge nodes on each lane increases as well. As a result, the interference at a serving edge node increases, which decreases the successful receiving probability of the serving edge node and thus increases the uplink local delay.

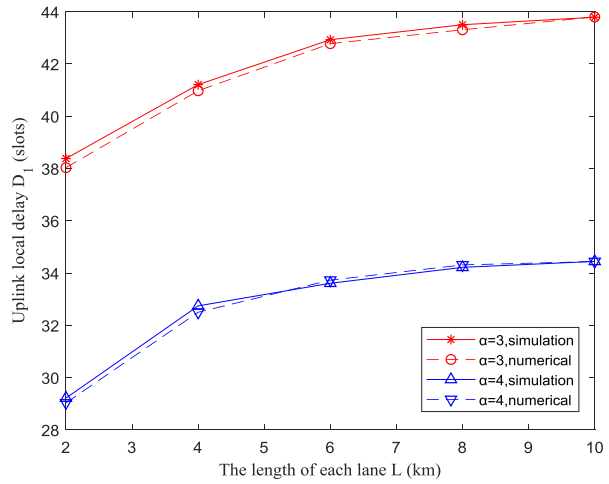

Fig. 12. Uplink local delay D_1 vs the length of each lane L ($\theta = 10$ dB, $\lambda_e = 0.025, \lambda_v^1 = 0.03, \lambda_v^2 = 0.02$).

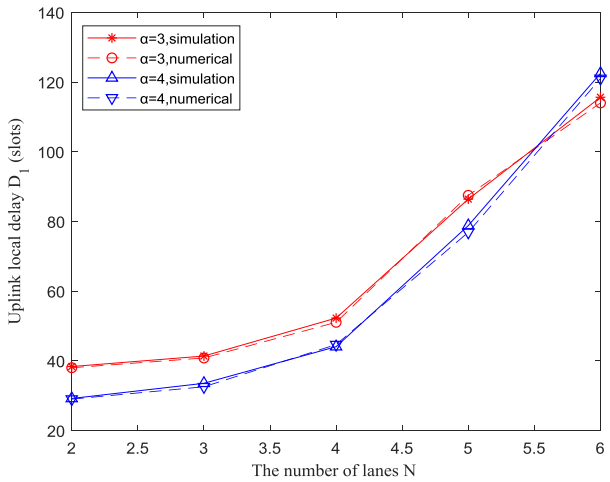

Fig. 13. Uplink local delay D_1 vs the number of lanes N. ($\theta = 10$ dB, $\lambda_e = 0.025, \lambda_v^1$=0.03, λ_v^2=0.02, λ_v^3=0.025, λ_v^4=0.035, λ_v^5=0.03, λ_v^6=0.025).

Fig. 13 shows the uplink local delay as a function of the number of lanes (N) when $\alpha = 3$ and $\alpha = 4$, respectively. It is seen that given the value of α, and the values of λ_e, λ_v^1, and λ_v^2, the local delay increases as N increases. This is because in this case as N increases the interference at a serving edge node increases, which decreases the successful receiving probability of a serving edge node. Meanwhile, as N increases, the number of vehicle nodes and edge nodes contending for the channel increases, which decreases the channel access probability of a service requesting vehicle. As a result, the local delay increases.

VI. Conclusion

In this paper, we studied the analysis of the uplink local delay in an MEC-based VANET and derived an analytical model based on stochastic geometry for analyzing the average uplink local delay of a vehicle driving on a highway for sending a packet to its serving edge node along the highway. In deriving the model, the spatial distributions of vehicles and edge nodes were modeled as an independent 1-D (PPP), respectively. A nearest-receiver model was used to determine the edge node for accommodating the service request of a vehicle node. Moreover, a CSMA mechanism was considered for channel access in the derived local delay model, which is more typical for a VANET. The derived analytical model was validated through simulation results and the impacts of major parameters on the average uplink local delay were investigated. The derived model is useful to parameter settings for the deployment of edge nodes. For future work, we will consider the extension of the derived local delay model taking into account the hidden-node problem avoidance in the network.

References

[1] J. Wang, J. Liu, and N. Kato, "Networking and communications in autonomous driving: A survey," *IEEE Commun. Surveys Tut.*, vol. 21, no. 2, pp. 1243–1274, Jun. 2019.
[2] F. Tang, Y. Kawamoto, N. Kato, and J. Liu, "Future intelligent and secure vehicular network towards 6G: Machine learning approaches," *Proc. IEEE*, vol. 108, no. 2, pp. 292–307, Feb. 2020, doi: 10.1109/JPROC.2019.2954595.
[3] Y. Wang, J. Zheng, and N. Mitton, "Delivery delay analysis for roadside unit deployment in vehicular ad hoc networks with intermittent connectivity," *IEEE Trans. Veh. Technol.*, vol. 65, no. 10, pp. 8591–8602, Oct. 2016.
[4] Y. Wang and J. Zheng, "Connectivity analysis of a highway with one entry/exit and multiple roadside units," *IEEE Trans. Veh. Technol.*, vol. 67, no. 12, pp. 11705–11718, Dec. 2018.
[5] J. Zheng and Y. Wang, "Connectivity analysis of vehicles moving on a highway with one entry and exit," *IEEE Trans. Veh. Technol.*, vol. 67, no. 5, pp. 4476–4486, May 2018.
[6] K. Zhang, Y. Mao, S. Leng, Y. He, and Y. Zhang, "Mobile-edge computing for vehicular networks: A promising network paradigm with predictive off-loading," *IEEE Veh. Technol. Mag.*, vol. 12, no. 2, pp. 36–44, Jun. 2017.
[7] H. Guo, J. Zhang, and J. Liu, "FiWi-enhanced vehicular edge computing networks: Collaborative task offloading," *IEEE Veh. Technol. Mag.*, vol. 14, no. 1, pp. 45–53, Mar. 2019.
[8] H. Guo and J. Liu, "Collaborative computation offloading for multi-access edge computing over fiber-wireless networks," *IEEE Trans. Veh. Technol.*, vol. 67, no. 5, pp. 4514–4526, May 2018.
[9] T. X. Tran and D. Pompili, "Joint task offloading and resource allocation for multi-server mobile-edge computing networks," *IEEE Trans. Veh. Technol.*, vol. 68, no. 1, pp. 856–868, Jan. 2019.
[10] C. Wang, F. R. Yu, and C. Liang, "Joint computation offloading and interference management in wireless cellular networks with mobile edge computing," *IEEE Trans. Veh. Technol.*, vol. 66, no. 8, pp. 7432–7445, Aug. 2017.
[11] H. Guo, J. Liu, J. Zhang, W. Sun, and N. Kato, "Mobile-edge computation offloading for ultra-dense IoT networks," *IEEE Internet Things J.*, vol. 5, no. 6, pp. 4977–4988, Dec. 2018.
[12] W. Na *et al.*, "Frequency resource allocation and interference management in mobile edge computing for an Internet of Things system," *IEEE Internet Things J.*, vol. 6, no. 3, pp. 4910–4920, Jun. 2019.
[13] H. Guo, J. Zhang, J. Liu, and H. Zhang, "Energy-aware computation offloading and transmit power allocation in ultra-dense IoT networks," *IEEE Internet Things J.*, vol. 6, no. 3, pp. 4317–4329, Jun. 2019.
[14] K. Rodrigues, K. Suto, and N. Kato, "Edge cloud server deployment with transmission power control through machine learning for 6G internet of things," *IEEE Trans. Emerg. Topics Comput.*, to be published, doi: 10.1109/TETC.2019.2963091.
[15] F. Baccelli and B. Blaszczyszyn, "A new phase transitions for local delays in MANETs," in *Proc. IEEE INFOCOM*, San Diego, CA, 2010, pp. 1–9.
[16] M. Haenggi, "The local delay in Poisson networks," *IEEE Trans. Inf. Theory*, vol. 59, no. 3, pp. 1788–1802, Mar. 2013.
[17] Z. Gong and M. Haenggi, "The local delay in mobile poisson networks," *IEEE Trans. Wireless Commun.*, vol. 12, no. 9, pp. 4766–4777, Sep. 2013.
[18] W. Nie, Y. Zhong, F. Zheng, W. Zhang, and T. O'Farrell, "HetNets with random DTX scheme: Local delay and energy efficiency," *IEEE Trans. Veh. Technol.*, vol. 65, no. 8, pp. 6601–6613, Aug. 2016.

[19] M. Salehi, A. Mohammadi, and M. Haenggi, "Analysis of D2D underlaid cellular networks: SIR meta distribution and mean local delay," *IEEE Trans. Commun.*, vol. 65, no. 7, pp. 2904–2916, Jul. 2017.
[20] L. Liu, Y. Zhong, W. Zhang, and M. Haenggi, "On the impact of coordination on local delay and energy efficiency in Poisson networks," *IEEE Wireless Commun. Lett.*, vol. 4, no. 3, pp. 241–244, Jun. 2015.
[21] M. Haenggi, "Local delay in static and highly mobile Poisson networks with ALOHA," in *Proc. IEEE Int. Conf. Commun. (ICC 2010)*, Cape Town, 2010, pp. 1–5.
[22] X. Dong, F. Zheng, R. Liu, and X. Zhu, "On the local delay and energy efficiency of HetNets with user mobility," in *Proc. IEEE Int. Conf. Commun. (ICC 2018)*, Kansas City, MO, 2018, pp. 1–6.
[23] F. Baccelli and B. Błaszczyszyn, *Stochastic Geometry and Wireless Networks, Volume II — Applications*. Foundations and Trends in Networking. Delft, The Netherlands: NoW Publishers, 2009.
[24] T. V. Nguyen, F. Baccelli, K. Zhu, S. Subramanian, and X. Wu, "A performance analysis of CSMA based broadcast protocol in VANETs," in *Proc. IEEE INFOCOM*, Turin, 2013, pp. 2805–2813.
[25] M. Haenggi, *Stochastic Geometry for Wireless Networks*. Cambridge, U.K.: Cambridge Univ. Press, 2012.
[26] H. Q. Nguyen, F. Baccelli, and D. Kofman, "A stochastic geometry analysis of dense IEEE 802.11 networks," in *Proc. IEEE INFOCOM*, Barcelona, Spain, 2007, pp. 1199–1207.
[27] R. K. Ganti and M. Haenggi, "Asymptotics and approximation of the SIR distribution in general cellular networks," *IEEE Trans. Wireless Commun.*, vol. 15, no. 3, pp. 2130–2143, Mar. 2016.

Yuying Wu received the bachelor's degree from the Nanjing University of Aeronautics and Astronautics, Nanjing, China, in 2016. She is currently working toward the Ph.D. degree with the School of Information Science and Engineering, Southeast University, Nanjing, China. Her research interests are in the area of edge computing and vehicular ad hoc networks, focusing on performance modeling and analysis. She has coauthored six conference papers.

Jun Zheng (Senior Member, IEEE) received the Ph.D. degree in electrical and electronic engineering from The University of Hong Kong, Hong Kong, in 2000. He is currently a Full Professor with the School of Information Science and Engineering, Southeast University (SEU), Nanjing, China. Before joining SEU in 2008, he was with the School of Information Technology and Engineering, University of Ottawa, Canada. He has coauthored (first author) two books published by Wiley-IEEE Press, and has coauthored nearly 200 technical papers in refereed journals and peer-reviewed conference proceedings. His current research interests include vehicular ad hoc networks, mobile communication networks, wireless sensor networks, focused on network architectures and protocols. He was the corecipient of an ICC 2014 Best Paper Award, a WCSP 2018 Best Paper Award, and a WiCON 2017 Best Student Paper Award. He serves as a Technical Editor for the *IEEE Communications Magazine* and was the Editor-in-Chief of *EAI Endorsed Transactions on Mobile Communications and Applications*. He is also an editorial board member of several refereed journals. He has coedited 12 special issues for different refereed journals and magazines, including the *IEEE Communications Magazine*, IEEE NETWORK, and IEEE JOURNAL ON SELECTED AREAS IN COMMUNICATIONS, all as a Lead Guest Editor. He was the founding General Chair of AdHocNets'09, a General Chair of AccessNets'07 and AdHocNets'18-19, and a TPC or Symposium Co-Chair for a number of international conferences and symposia, including IEEE ICC (2009, 2011, 2015, and 2021) and GLOBECOM (2008, 2010, 2012, 2018, and 2019). He has also served as a Technical Program Committee Member for a number of international conferences and symposiums. He is a Senior Member of the IEEE Communications Society, and IEEE Vehicular Technology Society. He also serves as Chair of IEEE Vehicular Technology Society Nanjing Chapter, and Chair of IEEE ComSoc Communications Switching and Routing Technical Committee.